

# Ultralow loss torsion micropendula for chip-scale gravimetry

C. A. Condos,<sup>1</sup> J. R. Pratt,<sup>2</sup> J. Manley,<sup>1</sup> A. R. Agrawal,<sup>1</sup> S. Schlamminger,<sup>2</sup> C. M. Pluchar,<sup>1</sup> and D. J. Wilson<sup>1</sup>

<sup>1</sup>Wyant College of Optical Sciences, University of Arizona, Tucson, AZ 85721, USA

<sup>2</sup>National Institute of Standards and Technology, 100 Bureau Drive, Gaithersburg, MD 20899

(Dated: November 7, 2024)

The pendulum is one of the oldest gravimeters, featuring frequency-based readout limited by geometric non-linearity. While modern gravimeters focus on displacement-based spring-mass or free-fall designs, the advent of nanofabrication techniques invites a revisiting of the pendulum, motivated by the prospect of low-loss, compact, isochronous operation, leveraging precise dimensional control. Here we exploit advances in strain-engineered nanomechanics—specifically, strained  $\text{Si}_3\text{N}_4$  nanoribbon suspensions—to realize a 0.1 mg, 32 Hz torsion pendulum with an ultralow damping rate of 16  $\mu\text{Hz}$  and a parametric gravity sensitivity of 5  $\text{Hz}/g_0$  ( $g_0 = 9.8 \text{ m/s}^2$ ). The low thermal acceleration of the pendulum,  $2 \times 10^{-9} g_0/\sqrt{\text{Hz}}$ , gives access to a parametric gravity resolution of  $10^{-8} g_0$  for drive amplitudes of 10 mrad and integration times within the free decay time, of interest for both commercial applications and fundamental experiments. We present progress toward this goal, demonstrating free and self-sustained oscillators with frequency stabilities as little as 2.5  $\mu\text{Hz}$  at 200 s, corresponding to a gravity resolution of  $5 \times 10^{-7} g_0$ . We also show how the Duffing nonlinearity of the suspension can be used to cancel the pendulum nonlinearity, paving the way toward a fully isochronous, high- $Q$  micromechanical clock.

Detecting gravity with small test masses is a key program for commercial technology and fundamental physics, and enjoys a rich history of innovation [1]. Recent advances have enabled micro-electromechanical (MEMS) gravimeters capable of detecting the earth's tides [2, 3], paving the way for applications such as low-cost geophysical surveys [4] and inertial navigation systems [5]. At a different extreme, micro-optomechanical systems (MOMS) have been used to detect the gravity of sub-100-mg test masses [6], and to prepare mechanical oscillators in their motional ground state [7]. Combining these abilities would enable long-standing proposals to search for new physics at the classical-quantum boundary [8].

In devising new strategies to miniaturize gravimeters, trade-offs exist between accuracy and sensitivity, practicality and extensibility. Tethered spring-mass systems are the most popular MEMS accelerometer platform because of their compatibility with wafer-scale fabrication and low noise capacitive readout; however, gravimetry-grade devices rely on complex nonlinear springs [2], and capacitive displacement measurements challenging to calibrate [9]. Conversely, fundamental experiments have driven a push to levitated test masses [10]. A key advantage of this approach is reduction of mechanical dissipation [11, 12], enhancing force sensitivity, and enabling quantum state preparation [7]. The practical demands of levitation however pose an impediment to commercialization.

Here we explore an approach to chip-scale gravimetry that combines virtues of tethered and levitated systems and may hold potential for both commercial and fundamental applications—based on an ultralow loss, lithographically-defined torsion micropendulum [13]. Torsion balances and pendula loom large in the history of gravimetry [14], in part because they can simulate free-fall for a few degrees of freedom. Moreover, pendula—arguably the first type of gravimeter [15, 16]—encode gravity into a frequency, which has distinct advantages over displacement metrology. Translating these advantages to chip-scale devices requires careful consideration of the hierarchy between external and internal stresses in nanoscale suspensions [17, 18], and how these can be leveraged to preserve sensitivity while reducing mass.

A key insight of our approach, described in [13], is that tensile stress can be used to stiffen a ribbon-like torsion suspension without adding loss. By suspending a Si microchip from a high-stress  $\text{Si}_3\text{N}_4$  nanoribbon—as shown in Fig. 1—we have realized a 0.1 mg torsion oscillator for which the hierarchy of gravitational ( $k_g$ ), tensile ( $k_\sigma$ ) and elastic ( $k_E$ ) stiffness is  $k_g \approx k_\sigma \approx 10^3 k_E$ . In this regime, the oscillator's parametric sensitivity to gravity is near that of an ideal pendulum  $\partial\omega/\partial g \approx \omega/g$ , while at the same time its quality factor ( $Q$ ) is dramatically increased, by dissipation dilution [18], to  $Q \approx Q_0(k_g + k_\sigma)/k_E > 10^6$ , where  $Q_0^{-1}$  is the loss tangent

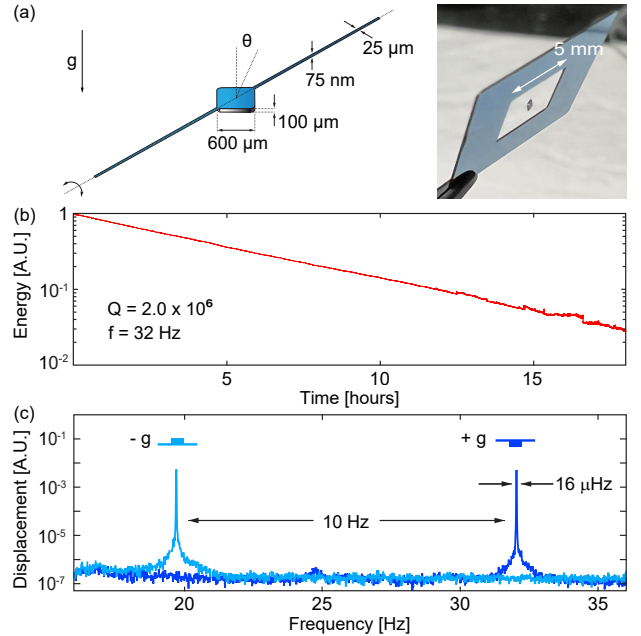


FIG. 1. **Chipscale torsion micropendulum.** (a) Illustration (left) and photo (right) of a pendulum formed by suspending a 0.1 mg Si mass from a 75 nm thick  $\text{Si}_3\text{N}_4$  nanoribbon. (b) Energy ringdown revealing a quality factor of approximately 2 million. (c) Displacement spectrum of inverted (dark blue) and normal (light blue) device with frequency  $\omega_- = 2\pi \times 20 \text{ Hz}$  and  $\omega_+ = 2\pi \times 32 \text{ Hz}$ , respectively.

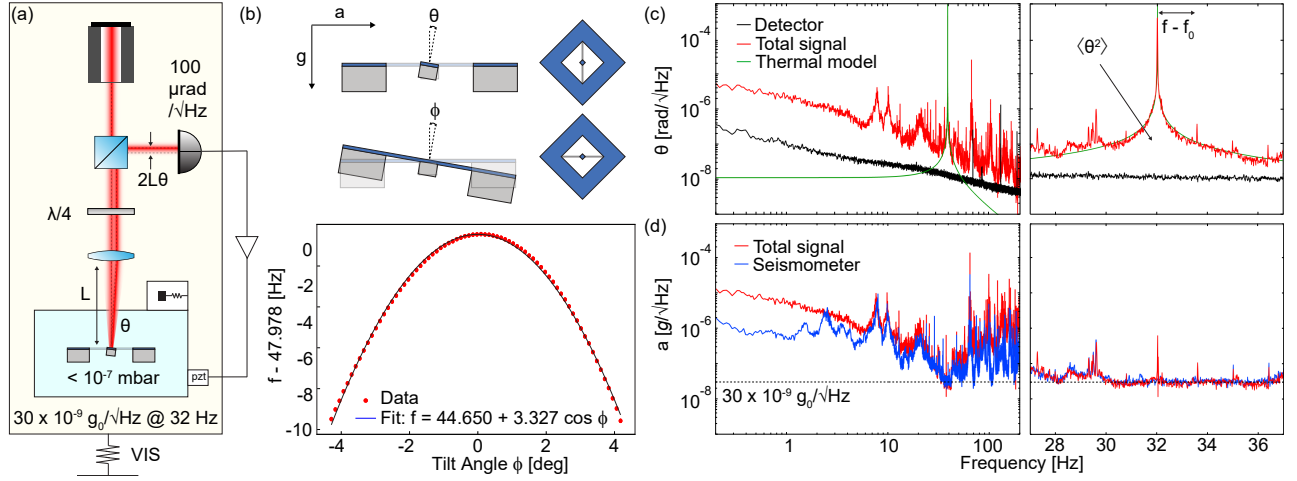


FIG. 2. (a) Overview of the experiment: The micropendulum is housed in a vacuum chamber (blue) mounted atop a vibration isolation system (VIS). Angular displacement  $\theta$  is probed with an optical lever (lever arm  $L = 3$  cm), optionally providing feedback via a piezo (“pzt”). All elements are housed in an opaque enclosure (yellow). (b) Tilt angle of pendulum ( $\theta$ ) and device chip ( $\phi$ ) relative to gravity  $g$  and horizontal acceleration  $a$  (top). Frequency versus device tilt angle illustrating the nonlinear stiffness of the pendulum (bottom). (c) Apparent displacement and (d) acceleration of the pendulum in its free-running state, compared to thermal noise models and an independent seismometer measurement.

of the suspension material. As visualized in Fig. 1c by inverting one device, the combined high sensitivity and  $Q$  yields a damping-rate-equivalent (spectral) gravity resolution of  $\Delta g \sim g/Q \approx 1 \times 10^{-6} g_0$  ( $g_0 = 9.80665 \text{ m/s}^2$  is the standard value of acceleration due to Earth [19]), an intriguing starting point for gravimetry experiments. In principle, moreover, the softening nonlinearity of gravity  $k_g'' < 0$  can be balanced against the hardening nonlinearity of the ribbon  $k_E'' > 0$ , yielding the prospect of an isochronous, high- $Q$  micromechanical clock.

In this Letter, we describe a set of experiments exploring the potential of our chipscale torsion micropendula as parametric (clock) gravimeters. Our near term goal is a semi-absolute gravimeter with a bias stability of  $10^{-7} g_0$ , sufficient to detect metrologically useful signals such as the tides or an altitude change of 1 meter. At the same time, the ability to detect gravity with a test mass on the order of the Planck mass ( $22 \mu\text{g}$ ) opens intriguing opportunities for fundamental physics experiments, ranging from searches for Yukawa-like forces [20] to tests of gravitational wavefunction collapse [21, 22].

The workhorse for our experiments is the device pictured in Fig. 1—a replica of the device studied in [13]—consisting of a  $0.6 \times 0.6 \times 0.1 \text{ mm}^3$  Si paddle suspended from a  $75 \text{ nm} \times 25 \mu\text{m} \times 7 \text{ mm}$   $\text{Si}_3\text{N}_4$  nanoribbon. The device possesses a resonance frequency, quality factor, and gravity sensitivity of  $\omega_0 = 2\pi \times 32 \text{ Hz}$ ,  $Q = 2 \times 10^6$ , and  $R = 2\pi \times 5 \text{ Hz}/g_0$ , respectively, corresponding to a damping rate of  $\gamma = \omega_0/Q = 2\pi \times 16 \mu\text{Hz}$  and a spectral resolution  $\Delta g = R^{-1}\gamma = 4 \times 10^{-6} g_0$ . For all experiments, the device is housed in a vacuum chamber ( $< 10^{-8}$  mbar) atop a passive vibration isolation system tuned so that its transmissibility is minimal at  $\omega_0$ . Angular displacement is recorded using a low noise optical lever [13].

Our main aim is to explore the bias stability  $\sigma_g$  of the micropendulum operated as a clock gravimeter. In the limit that the frequency stability is thermal noise limited ( $\sigma_\omega = \sqrt{\gamma/(2\varepsilon\tau)}$  [23]),  $\sigma_g$  can be expressed as an Allan deviation

$$\sigma_g = R^{-1} \sigma_\omega = \Delta g / \sqrt{2\varepsilon\gamma\tau} \quad (1)$$

where  $\tau$  is the integration time and  $\varepsilon = \theta_0^2 / \langle \theta_{\text{th}}^2 \rangle$  is the ratio of the coherent and thermal displacement power [23]. Eq. 1 suggests that for a clock gravimeter with a spectral resolution  $\Delta g = 5 \times 10^{-6} g_0$ , a bias stability of  $\sigma_g \approx 10^{-7} g_0$  is possible by averaging over 100 coherence times  $\gamma^{-1}$ ; or in a single coherence time if the oscillator is driven to an amplitude 100-times in excess of thermal noise. Leveraging these tradeoffs involves considering extraneous noise, drift, and nonlinearities, all of which can be large for nanomechanical devices.

As a starting point, we revisit the measurement shown in Fig. 1c, in which the parametric gravity sensitivity  $R$  of the pendulum is visualized by comparing its frequency in normal  $\omega_0 = \omega_+$  and inverted  $\omega_0 = \omega_-$  chip orientations. The change in frequency reveals the fraction of the pendulum’s total stiffness  $k_{\text{tot}} \propto \omega_0^2$  which is due to gravity, which depends in turn on the direction of gravity relative to the torsion paddle, viz.

$$k_{\text{tot}}(\phi) = k_g \cos(\phi) + k_\sigma + k_E$$

$$R(\phi) = \frac{\partial \omega_0(\phi)}{\partial g} \lesssim \frac{\omega_+^2 - \omega_-^2}{4g\omega_+} \approx \frac{\omega_+ - \omega_-}{2g}, \quad (2)$$

where  $\phi$  is the chip tilt angle, defined such that  $\omega_0(0) = \omega_+$  and  $\omega_0(\pi) = \omega_-$  (see Fig. 2b). Eq. 2 allows us to directly calibrate the parametric sensitivity of the pendulum, yielding  $R(0) = 2\pi \times 5 \text{ Hz}/g_0$  in its normal orientation. It also highlights the fact that a pendulum is intrinsically nonlinear. We visualize this in Fig. 2b by tracking the frequency of a similar device versus  $\phi$  in an auxiliary,

A key assumption behind Eq. 1 is that displacement readout is thermal noise limited—i.e., thermal motion  $S_\theta^{\text{th}}(\Omega) \approx \langle \theta_{\text{th}}^2 \rangle \gamma / ((\Omega - \omega_0)^2 + \gamma^2/4)$  (expressed here as a one-sided power spectral density) exceeds readout noise  $S_\theta^{\text{imp}}$  at an offset frequency  $\Omega - \omega_0 \approx 2\pi/\tau$ , where  $\langle \theta_{\text{th}}^2 \rangle = k_B T_0 / (I\omega_0^2)$  and  $I \approx 2 \text{ pgm}^2$  are the thermal displacement variance and moment of inertia of the pendulum, respectively. To investigate this requirement, as shown in Fig. 2c, we probed the pen-

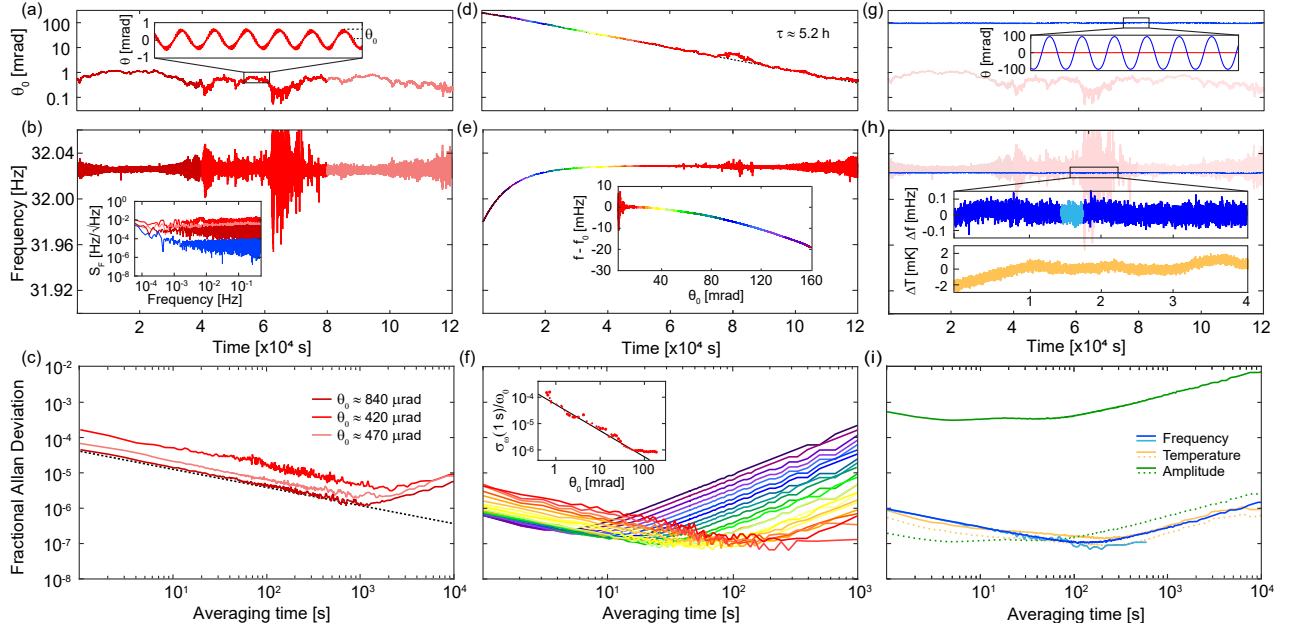


FIG. 3. **Micropendulum frequency stability.** (a) Amplitude of free-running pendulum over several hours. Inset: Instantaneous amplitude over several periods. (b) Corresponding frequency estimate. Inset: Frequency spectrum for highlighted intervals and data in (h) inset. (c) Fractional Allan Deviation (FAD) of data in (b). (d) Amplitude ringdown of transiently driven pendulum. (e) Frequency time series data concurrent with ringdown. Inset: Frequency shift versus amplitude. (f) FAD of successive 2000 s segments of the ringdown in (e). Inset: 1 s FAD versus amplitude. (g) Amplitude of pendulum driven into self-sustained oscillation (SSO) compared to the free-running pendulum (red). (h) Corresponding frequency estimate. Insets: Frequency (blue) and temperature (orange) versus time over highlighted  $4 \times 10^4$  s interval. (i) FAD of frequency, temperature and amplitude data in (h). Dashed lines are estimates of frequency-equivalent temperature and amplitude noise.

dulum with a  $10 \mu\text{W}$  optical lever, and found that readout noise  $S_{\theta}^{\text{imp}} \approx (0.1 \text{ mrad}/\sqrt{\text{Hz}})^2$  matched displacement noise at  $\Omega - \omega_0 \approx 2\pi \times 1\text{Hz}$ ; however, the calibrated noise variance  $\langle \theta^2 \rangle \approx (0.1 \text{ mrad})^2$  was larger than the expected thermal value  $\langle \theta_{\text{th}}^2 \rangle \approx (7 \mu\text{rad})^2$  by two orders of magnitude. This excess motion appears to stem from ambient lateral acceleration at the level of  $S_a(\omega_0) \approx (3 \times 10^{-8} g_0/\sqrt{\text{Hz}})^2$ , as evidenced in Fig. 2d by comparing seismometer data (blue) to an indirect calibration  $S_a(\omega_0) = (\langle \theta^2 \rangle / \langle \theta_{\text{th}}^2 \rangle) S_a^{\text{th}}$  (red), where  $S_a^{\text{th}} = 4k_B T \gamma l / (m r_{\text{CM}})^2 \approx (2 \times 10^{-9} g_0/\sqrt{\text{Hz}})^2$ ,  $m \approx 0.1 \text{ mg}$ ,  $r_{\text{CM}} \approx 50 \mu\text{m}$  are the acceleration-equivalent thermal noise, mass and lever arm of the pendulum, respectively. This discrepancy underscores the high acceleration sensitivity of the micropendulum, and implies that thermal displacement noise in Eq. 1 must be replaced by  $\langle \theta^2 \rangle \sim 10^2 \langle \theta_{\text{th}}^2 \rangle$ , while  $\tau^{-1/2}$  scaling should occur for averaging times  $\tau \gtrsim 1 \text{ s}$ .

Armed with these expectations, we conducted a series of experiments to determine the frequency stability of the micropendulum in Fig. 1. For these experiments, as illustrated in Fig. 2a, the apparatus was housed in an opaque enclosure and the device platform was temperature-stabilized to within approximately 1 mK using a Peltier cooler. The amplitude of the pendulum was controlled using active feedback of the optical lever photocurrent to a piezo affixed to the vacuum chamber. The frequency of the pendulum was estimated using a software fitting routine applied to the digitized photocurrent [13].

As shown in Fig. 3a, we first recorded the frequency of the pendulum in its free running state,  $\varepsilon = 1$ , sampling at 100 kHz for 1 second intervals. At short times, the frequency Allan deviation  $\sigma_{\omega}$  was found to scale in qualitative agreement

with the thermal noise model (Eq. 1). Beyond  $10^3$  seconds, frequency noise is overcome by linear drift  $\sigma_{\omega} \propto \tau$ . At least a fraction of this drift is due to temperature instability, as revealed by the reduction of  $\sigma_{\omega}$  after detrending by the peltier error signal. For the detrended data, we observe a minimum frequency stability of  $\sigma_{\omega} \approx 1.1 \times 10^{-6} \omega_0$  at  $\tau \approx 1500 \text{ s}$ , corresponding to a gravity resolution of  $\sigma_g \approx 7.0 \times 10^{-6} g_0$ .

According to Eq. 1, frequency stability can be increased by driving the pendulum into coherent oscillation,  $\varepsilon > 1$ , in principle realizing  $\sigma_g = 10^{-7} g_0$  within the coherence time  $\gamma^{-1} \approx 10^4 \text{ s}$ , if the pendulum nonlinearity is sufficiently low. To explore this possibility, we conducted an experiment in which the pendulum was transiently excited—using feedback as shown in Fig. 2—and then allowed to undergo free decay,  $\theta_0(t) = \theta_1 e^{-\gamma t/2}$ , resulting in a frequency ringdown [24]

$$\omega(t) \approx \omega_0 \left( 1 + \frac{k_g'' + k_E''}{16k_{\text{tot}}} \theta_1^2 e^{-2\gamma t} \right) \equiv \omega_0 (1 + \alpha_{\text{NL}} \theta_0^2(t)) \quad (3)$$

where  $k_g'' = -k_g$  and  $k_E''$  are the pendulum nonlinearity and suspension nonlinearity, respectively, and  $k_{\text{tot}} \approx k_{\sigma} + k_g$  is the total pendulum stiffness. For the measurement shown in Fig. 3e, the oscillator was driven to  $\theta_1 = 160 \text{ mrad}$  and  $\sigma_{\omega}$  was computed on  $\tau = 10^3 \text{ s}$  intervals. Evidently, driving produces the anticipated reduction of  $\sigma_{\omega}$  at short times; however, drift due to the pendulum nonlinearity  $\alpha_{\text{NL}} \approx 2 \times 10^{-8} / \text{mrad}^2$  fundamentally limits the frequency stability to  $\sigma_{\omega} \approx 2 \times 10^{-7} \omega_0$  at  $\tau \approx 10^2 \text{ s}$ , corresponding to  $\sigma_g = 1.3 \times 10^{-6} g_0$ .

To mitigate nonlinear frequency drift, we turned our attention to stabilizing the amplitude of the micropendulum. To

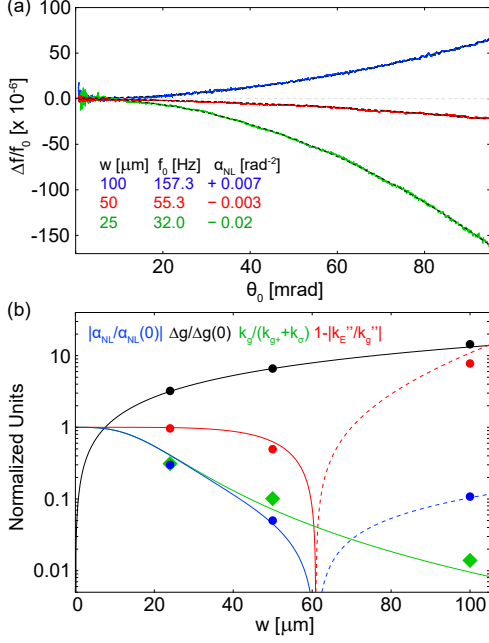


FIG. 4. **Towards an isochronous micropendulum.** (a) Frequency versus amplitude for micropendula with 25  $\mu\text{m}$ , 50  $\mu\text{m}$ , and 100  $\mu\text{m}$  wide suspensions. Dashed lines are quadratic fits. (b) Measurements (markers) and models (lines) of frequency nonlinearity  $\alpha_{\text{NL}}$  (blue), damping-equivalent gravity resolution  $\Delta g = R^{-1}f/Q$  (black), participation factor of gravitational stiffness  $k_g/k_{\text{tot}}$  (green), and relative nonlinearity  $|(k_g - k_E'')/k_g|$  (red). See main text for details.

this end, following a standard approach, we implemented a self-sustained oscillator by combining piezoelectric feedback with a gain-clamped amplifier. Shown in Fig. 3(g-i) is an experiment for which, after a settling time of several hours, the amplitude was stabilized to within 1% of  $\theta_0 \approx 100$  mrad. The frequency, amplitude, and temperature of the pendulum were then tracked for a day. Over the highlighted 11-hour period, we observed that the frequency stability of the pendulum was limited to  $\sigma_\omega \approx 1.1 \times 10^{-7} \omega_0$  at 100 s, corresponding to  $\sigma_g \approx 7 \times 10^{-7} g_0$ . Overlays of the temperature and amplitude AD scaled by the measured temperature sensitivity  $f^{-1} \partial f / \partial T \approx 4 \times 10^{-6} / \text{mK}$  [24] and amplitude sensitivity  $f^{-1} \partial f / \partial \theta_0 = 2\alpha_{\text{NL}} \theta_0 \approx 2 \times 10^{-6} / \text{mrad}$  suggest that temperature ( $\sigma_T \gtrsim 30$   $\mu\text{K}$ ) and amplitude noise ( $\sigma_{\theta_0} \gtrsim 40$   $\mu\text{rad}$ ) contribute equally to the observed instability. Over the highlighted, relatively stable, 20 min interval, we observe minima  $\sigma_\omega \approx 7 \times 10^{-8} \omega_0$  and  $\sigma_g \approx 5 \times 10^{-7} g_0$  at 200 s.

Our experiments suggest that the frequency stability of our torsion micropendulum is limited by environmental noise and drift—in particular, acceleration noise, temperature drift, and amplitude drift—limiting drive powers, integration times, frequency stability, and parametric gravity resolution to  $\varepsilon \approx 10^4$ ,  $\tau \approx 10^2$  s,  $\sigma_f \approx 1$   $\mu\text{Hz}$ , and  $\sigma_g \approx 10^{-6} g_0$ , respectively. They also highlight a fundamental tradeoff, in that leveraging high drive powers and integration times entails increased sensitivity to amplitude fluctuations due to the pendulum nonlinearity:

$$\sigma_\omega^2(\tau) \gtrsim \frac{\gamma\langle\theta_{\text{th}}^2\rangle}{2\theta_0^2\tau} + 4\alpha_{\text{NL}}^2\theta_0^2\sigma_{\theta_0}^2(\tau) \geq 4\alpha_{\text{NL}}\sqrt{\frac{2\tau\sigma_{\theta_0}^2(\tau)}{\gamma\langle\theta_{\text{th}}^2\rangle}} \quad (4)$$

The nonlinear instability given by Eq. 4 is a well-known limitation of pendulum clocks [1] dating back to Huygens, and poses a fundamental obstacle to pendulum-based sensors. However, the hierarchy of stiffnesses of our micropendula yields a surprising workaround, in that the gravitational nonlinearity  $k_g'' = -k_g$  is comparable but opposite in sign to the suspension nonlinearity  $k_E''$ , enabling cancellation of the net nonlinearity by tailoring the ribbon dimensions. Viz., [25]

$$\alpha_{\text{NL}} = \frac{-k_g}{16k_{\text{tot}}} \left(1 - \frac{k_E''}{k_g}\right) \approx \alpha_{\text{NL}}^0 \left(1 - \frac{3hw^5E}{5L^2mgr_{\text{CM}}}\right) \quad (5)$$

where  $\alpha_{\text{NL}}^0 = k_g/(16k_{\text{tot}})$  is the gravitational nonlinearity (1/16 for an ideal pendulum,  $k_{\text{tot}} = k_g$ ) and the  $k_E'' \approx 3Ehw^5/(5L^3)$  is the nonlinear torsional stiffness of a ribbon of thickness  $h$ , width  $w$ , and length  $L$  [24, 25]. Indeed, noting that the ribbon tensile stiffness  $k_\sigma = \sigma hw^3/6L$  and gravitational sensitivity  $R \propto (1 + k_\sigma/k_g)^{-1/2}$ , Eq. 5 implies that  $\alpha_{\text{NL}}$  can be cancelled without altering  $R$ , by tailoring  $w$  and  $r_{\text{CM}}$ .

To explore the possibility of cancelling the pendulum nonlinearity, we fabricated two additional pendula with suspension widths of  $w = 50$   $\mu\text{m}$  and  $100$   $\mu\text{m}$  (otherwise the pad dimensions were fixed), and compared their nonlinear ring-downs and gravity sensitivity to the  $w = 25$   $\mu\text{m}$  device. As shown in Fig. 4a, the magnitude of the nonlinearity was observed to decrease 10-fold for the 50  $\mu\text{m}$  device and change sign for the 100  $\mu\text{m}$  device. Meanwhile, the gravitational sensitivity exhibits the expected  $w^{-3/2}$  scaling. As shown in Fig 4b, this behavior is consistent with Eq. 5 using  $r_{\text{CM}} = 48$   $\mu\text{m}$  and  $m = 67$   $\mu\text{g}$ , which predicts  $\alpha_{\text{NL}} = 0$  for  $w \approx 60$   $\mu\text{m}$ .

In summary, we explored a new class of chip-scale pendulum gravimeters based on strained  $\text{Si}_3\text{N}_4$  nanoribbon suspensions [13]. Owing to their unique hierarchy of gravitational, tensile, and elastic stiffness, these devices possess  $Q$  factors exceeding  $10^6$  (via dissipation dilution), parametric gravity sensitivities ( $R$ ) approaching that of an ideal pendulum, and a route to isochronous operation by balancing the elastic and gravitational nonlinearity. As an illustration, we studied a 32 Hz, 0.1 mg pendulum with a damping rate of 16  $\mu\text{Hz}$  and  $R = 5$  Hz/ $g_0$ . Driven into self-sustained oscillation, we recorded Allan Deviations as low as 2.5  $\mu\text{Hz}$  at 200 seconds—corresponding to a gravity resolution of  $5 \times 10^{-7} g_0$ —limited by temperature, amplitude, acceleration noise at the level of 30  $\mu\text{K}$ , 50  $\mu\text{rad}$ , and  $10^{-7} g_0/\sqrt{\text{Hz}}$ , respectively. We also demonstrated a ten-fold cancellation of the pendulum nonlinearity by varying the width of the ribbon suspension.

Looking forward, we envision a combination of improved environmental control and isochronicity to achieve a resolution to gravity lower than  $10^{-7} g_0$ , sufficient for clock-based altimetry and tidal monitoring. A key challenge is dimensional control over the torsion paddle. To this end, we have recently developed a dry-etching procedure that achieves a 100 Hz pendulum with  $R = 4.4$  Hz/ $g_0$  and  $\alpha_{\text{NL}} \approx 0.0002$ , a 100-fold reduction over the device studied here. We also note that the observed frequency-temperature sensitivity of our device is 10-times larger than expected due to stress relaxation ( $\alpha_{\text{rel}}E/(2\sigma)$ , where  $\alpha_{\text{rel}}$  is the relative thermal expansion coefficient of Si and  $\text{Si}_3\text{N}_4$ ) [26], implying a significant margin for improvement using strain-engineering [26] or strained

Si ( $\alpha_{\text{rel}} = 0$ ) [27]. Finally, an important obstacle is the ultralow thermal acceleration and torque of the micropendula—approximately  $10^{-9}g_0/\sqrt{\text{Hz}}$  and  $10^{-19}\text{Nm}/\sqrt{\text{Hz}}$ , for the reported device—which requires careful vibration isolation at our current seismic frequencies. From a different perspective, these sensitivities suggest that our micropendula are promising as displacement based accelerometers. Indeed, they occupy a sensitivity regime for micromechanical oscillators typically reserved for levitated systems [12, 28], making them a

promising platform for proposals to search for new physics at the quantum-classical boundary [6, 8, 29, 30].

#### ACKNOWLEDGEMENTS

The authors thank Will Terrano for useful discussions. This work was supported by the National Science Foundation, awards 2239735 and 2330310. CAC acknowledges support from a UArizona National Labs Partnership Grant. ARA was supported by a CNRS-UArizona iGlobes Fellowship.

- 
- [1] I. Marson, “A short walk along the gravimeters path,” *Int. J. Geophys.* **2012** (2012).
- [2] R. Middlemiss, A. Samarelli, D. Paul, J. Hough, S. Rowan, and G. Hammond, “Measurement of the earth tides with a mems gravimeter,” *Nature* **531**, 614–617 (2016).
- [3] A. Mustafazade, M. Pandit, C. Zhao, G. Sobreviela, Z. Du, P. Steinmann, X. Zou, R. T. Howe, and A. A. Seshia, “A vibrating beam mems accelerometer for gravity and seismic measurements,” *Sci. Rep.* **10**, 10415 (2020).
- [4] D. Carbone, L. Antoni-Micollier, G. Hammond, E. de Zeeuw-van Dalssen, E. Rivalta, C. Bonadonna, A. Messina, J. Lautier-Gaud, K. Toland, M. Koymans, et al., “The newton-g gravity imager: toward new paradigms for terrain gravimetry,” *Frontiers in Earth Science* **8**, 573396 (2020).
- [5] N. El-Sheimy and A. Youssef, “Inertial sensors technologies for navigation applications: State of the art and future trends,” *Satellite Navigation* **1**, 2 (2020).
- [6] T. Westphal, H. Hepach, J. Pfaff, and M. Aspelmeyer, “Measurement of gravitational coupling between millimetre-sized masses,” *Nature* **591**, 225–228 (2021).
- [7] U. Delić, M. Reisenbauer, K. Dare, D. Grass, V. Vuletić, N. Kiesel, and M. Aspelmeyer, “Cooling of a levitated nanoparticle to the motional quantum ground state,” *Science* **367**, 892–895 (2020).
- [8] M. Rademacher, J. Millen, and Y. L. Li, “Quantum sensing with nanoparticles for gravimetry: when bigger is better,” *Advanced Optical Technologies* **9**, 227–239 (2020).
- [9] G. D’Emilia, A. Gaspari, F. Mazzoleni, E. Natale, and A. Schiavi, “Calibration of tri-axial mems accelerometers in the low-frequency range—part 1: comparison among methods,” *Journal of Sensors and Sensor Systems* **7**, 245–257 (2018).
- [10] C. Gonzalez-Ballester, M. Aspelmeyer, L. Novotny, R. Quidant, and O. Romero-Isart, “Levitodynamics: Levitation and control of microscopic objects in vacuum,” *Science* **374**, eabg3027 (2021).
- [11] J. Hofer, R. Gross, G. Higgins, H. Huebl, O. F. Klier, R. Kleiner, D. Koelle, P. Schmidt, J. A. Slater, M. Trupke, K. Uhl, T. Weimann, W. Wieczorek, and M. Aspelmeyer, “High- $q$  magnetic levitation and control of superconducting microspheres at millikelvin temperatures,” *Phys. Rev. Lett.* **131**, 043603 (2023).
- [12] L. Dania, D. S. Bykov, F. Goschin, M. Teller, A. Kassid, and T. E. Northup, “Ultrahigh quality factor of a levitated nanomechanical oscillator,” *Phys. Rev. Lett.* **132**, 133602 (2024).
- [13] J. R. Pratt, A. R. Agrawal, C. A. Condos, C. M. Pluchar, S. Schlamminger, and D. J. Wilson, “Nanoscale torsional dissipation dilution for quantum experiments and precision measurement,” *Phys. Rev. X* **13**, 011018 (2023).
- [14] G. T. Gillies and R. C. Ritter, “Torsion balances, torsion pendulums, and related devices,” *Rev. Sci. Instrum.* **64**, 283 (1993).
- [15] J. Richer, “Observations astronomiques et physiques faites en l’isle de caïenne,” *Observations astronomiques et physiques faites en l’isle de Caïenne* (1731).
- [16] D. C. Agnew, “Time and tide: pendulum clocks and gravity tides,” *History of Geo-and Space Sciences* **11**, 215–224 (2020).
- [17] R. Shaniv, S. K. Keshava, C. Reetz, and C. A. Regal, “Understanding the quality factor of mass-loaded tensioned resonators,” *Physical Review Applied* **19**, L031006 (2023).
- [18] L. Sementilli, E. Romero, and W. P. Bowen, “Nanomechanical dissipation and strain engineering,” *Advanced Functional Materials* **32**, 2105247 (2022).
- [19] E. Tiesinga, P. J. Mohr, D. B. Newell, and B. N. Taylor, “CODATA recommended values of the fundamental physical constants: 2018,” *J. Phys. Chem. Ref. Data* **50** (2021).
- [20] E. Adelberger, B. Heckel, and A. Nelson, “Tests of the gravitational inverse-square law,” *Annu. Rev. Nucl. Part. Sci.* **53**, 77–121 (2003).
- [21] A. Bassi, K. Lochan, S. Satin, T. P. Singh, and H. Ulbricht, “Models of wave-function collapse, underlying theories, and experimental tests,” *Rev. Mod. Phys.* **85**, 471 (2013).
- [22] S. Kryhin and V. Sudhir, “Distinguishable consequence of classical gravity on quantum matter,” *arXiv preprint arXiv:2309.09105* (2023).
- [23] M. Wang, R. Zhang, R. Ilic, , and V. A. Aksyuk, “Fundamental limits and optimal estimation of the resonance frequency of a linear harmonic oscillator,” *Commun. Phys.* **4**, 207 (2021).
- [24] “Supplementary information,” See Supplementary Information.
- [25] J. R. Pratt, S. Schlamminger, A. R. Agrawal, C. A. Condos, C. M. Pluchar, and D. J. Wilson, “The intersection of noise, amplitude, and nonlinearity in a high- $q$  micromechanical torsion pendulum,” in *ICND* (Springer, 2023) pp. 3–14.
- [26] M. Wang, R. Zhang, R. Ilic, V. Aksyuk, and Y. Liu, “Frequency stabilization of nanomechanical resonators using thermally invariant strain engineering,” *Nano letters* **20**, 3050–3057 (2020).
- [27] A. Beccari, D. A. Visani, S. A. Fedorov, M. J. Beryhi, V. Boureau, N. J. Engelsens, and T. J. Kippenberg, “Strained crystalline nanomechanical resonators with quality factors above 10 billion,” *Nature Physics* **18**, 436–441 (2022).
- [28] C. W. Lewandowski, T. D. Knowles, Z. B. Etienne, and B. D’Urso, “High-sensitivity accelerometry with a feedback-cooled magnetically levitated microsphere,” *Physical Review Applied* **15**, 014050 (2021).
- [29] J. Manley, C. Condos, S. Schlamminger, J. Pratt, D. Wilson, and W. Terrano, “Microscale torsion resonators for short-range gravity experiments,” *arXiv preprint arXiv:2406.13020* (2024).
- [30] D. C. Moore and A. A. Geraci, “Searching for new physics using optically levitated sensors,” *Quantum Sci. Technol.* **6**, 014008 (2021).

# Supplementary information for “Ultralow loss torsion micropendula for chip-scale gravimetry”

C. A. Condos,<sup>1</sup> J. R. Pratt,<sup>2</sup> J. Manley,<sup>1</sup> A. R. Agrawal,<sup>1</sup> S. Schlamminger,<sup>2</sup> C. M. Pluchar,<sup>1</sup> and D. J. Wilson<sup>1</sup>

<sup>1</sup>Wyant College of Optical Sciences, University of Arizona, Tucson, AZ 85721, USA

<sup>2</sup>National Institute of Standards and Technology, 100 Bureau Drive, Gaithersburg, MD 20899

(Dated: November 7, 2024)

arXiv:2411.04113v1 [physics.app-ph] 6 Nov 2024

## NONLINEAR DYNAMICS OF A TORSION PENDULUM

Consider a simple pendulum of mass  $m$  and length  $r$  which is constrained to oscillate in a plane at tilted  $\phi$  from the gravitation field (such that  $\phi = 0$  for a standard pendulum and  $\phi = \pi$  for an inverted pendulum). When displaced by  $\theta$  from rest, the pendulum experiences a nonlinear restoring torque

$$\tau_g(\theta) = mgr \cos \phi \sin \theta \quad (\text{S1})$$

or equivalently, a nonlinear stiffness

$$k_g(\theta) \equiv \tau'_g(\theta) = mgr \cos \phi \cos \theta \quad (\text{S2})$$

Expanding about  $\theta = 0$  to third order gives

$$\tau(\theta) \approx -k_g \theta - k''_g \theta^3 / 6 \quad (\text{S3})$$

where for notational simplicity we define

$$\begin{aligned} k_g &= k_g(0) = mgr \cos \phi \\ k''_g &= k''_g(0) = -k_g \end{aligned} \quad (\text{S4})$$

as the linear spring constant ( $k_g$ ) and second order (Duffing) nonlinearity ( $k''_g$ ) of the pendulum, respectively.

Now consider a torsion pendulum which is subject to an additional restoring torque from its suspension. For a ribbon suspension with tensile stress  $\sigma$  and elastic modulus  $E$  the additional linear and nonlinear torsional stiffnesses are [1]

$$\begin{aligned} k_\sigma &= \frac{\sigma h w^3}{3L} \\ k''_\sigma &= -\frac{3\sigma h w^5}{5L^3} \\ k_E &= \frac{2E h^3 w}{3L} \\ k''_E &= \frac{3E h w^5}{5L^3} \end{aligned} \quad (\text{S5})$$

where  $w$ ,  $L$ ,  $h$  are the ribbon width, length, and thickness, respectively. For the torsion micropendula presented in the main text,  $|k''_\sigma| \ll |k''_E|$  and  $k_E \ll k_\sigma$ . The net (total) linear and nonlinear torsional stiffnesses can therefore be expressed as

$$\begin{aligned} k_{\text{tot}} &= k_\sigma + k_E + k_g \approx k_\sigma + k_g \\ k''_{\text{tot}} &= k''_\sigma + k''_E + k''_g \approx k''_E + k''_g \end{aligned} \quad (\text{S6})$$

## Frequency-amplitude coupling

The torsion micropendula presented in the main text can be modeled with the nonlinear (Duffing) equation of motion

$$I \ddot{\theta} + k_{\text{tot}} \theta + \frac{k''_{\text{tot}}}{6} \theta^3 = 0 \quad (\text{S7})$$

where  $I$  is the moment of inertia of the torsion paddle and  $k_{\text{tot}}$  and  $k''_{\text{tot}}$  are as given by Eq. S6.

The solution to Eq. S7 is well known [2]. For a sufficiently small initial amplitude  $\theta_0$ , a stable orbit with a period

$$T(\theta_0) \approx \frac{2\pi}{k_{\text{tot}}/I} \left( 1 - \frac{3}{8} \frac{\beta}{\omega_1^2} \theta_0^2 \right) \quad (\text{S8})$$

is described, corresponding to an effective frequency

$$\omega(\theta_0) \equiv \frac{2\pi}{T(\theta_0)} \approx \omega_0 (1 + \alpha_{\text{NL}} \theta_0^2) \quad (\text{S9})$$

where  $\omega_0 = \sqrt{k_{\text{tot}}/I}$  is the “cold” frequency and

$$\alpha_{\text{NL}} \equiv \frac{1}{16} \frac{k''_{\text{tot}}}{k_{\text{tot}}}. \quad (\text{S10})$$

Equation S10 describes the frequency-amplitude coupling of the torsion pendulum. It vanishes when  $k''_{\text{tot}} = 0$  (i.e., when  $k_E + k_\sigma = -k_g$ ), a condition known as “isochronous.”

## Parametric sensitivity to gravity

Because the magnitude of  $\tau_g$  depends on local gravitational acceleration  $g$ , the pendulum oscillation frequency is sensitive to changes in  $g$ . The sensitivity is given by

$$R \equiv \frac{\partial \omega_0}{\partial g} = \frac{\omega_0}{2g} \frac{k_g}{k_{\text{tot}}} \quad (\text{S11})$$

## Calibration of $R$ and $\alpha_{\text{NL}}$ via device inversion

In the case relevant to the main text— $\phi = 0$ ,  $\kappa_E \ll k_g$ , and  $k_E \ll k_\sigma$ —both  $R$  and  $\alpha_{\text{NL}}$  can be expressed in terms of the non-inverted  $\omega_0(\phi = 0) = \sqrt{(k_\sigma + k_g)/I} \equiv \omega_+$  and inverted  $\omega_0(\phi = \pi) = \sqrt{(k_\sigma - k_g)/I} \equiv \omega_+$  pendulum frequency,

$$R \approx \frac{\omega_+^2 - \omega_-^2}{4g\omega_+} = \frac{8\alpha_{\text{NL}}}{g}, \quad (\text{S12})$$

highlighting a fundamental sensitivity-nonlinearity tradeoff.

## FREQUENCY STABILITY

The frequency stability of a linear oscillator is fundamentally limited by thermal noise, modeled by the Allan deviation

$$\sigma_{\omega}^{\text{th}}(\tau) \approx \sqrt{\frac{\omega_0}{2Q\varepsilon\tau}} \quad (\text{S13})$$

where  $\varepsilon = \langle \theta^2 \rangle / \theta_{\text{th}}^2 = \theta_0^2 / (2\theta_{\text{th}}^2)$  is the ratio of the average oscillator energy to the thermal energy [3–5]. Evidently, frequency noise can be reduced by coherently driving the oscillator. However, for a nonlinear oscillator, this advantage is countered by increased sensitivity to amplitude fluctuations (Eq. S15). Specifically, for small amplitude fluctuations  $\sigma_{\theta_0}$  about a drive amplitude  $\theta_0$ , one might anticipate

$$\sigma_{\omega}^{\text{NL}} \approx \left| \frac{\partial \omega}{\partial \theta_0} \right| \sigma_{\theta_0} = 2\omega_0 \alpha_{\text{NL}} \theta_0 \sigma_{\theta_0}, \quad (\text{S14})$$

implying the existency of a critical amplitude at which the advantage of increasing  $\theta_1$  is saturated.

### Frequency drift in free decay

Figure 3e shows the frequency drift of a micropendulum during an amplitude ringdown  $\theta_0(t) = \theta_1 e^{-\gamma t/2}$ , exhibiting an exponential decay due to amplitude-frequency coupling:

$$\omega(t) \approx \omega_0 (1 + \alpha_{\text{NL}} \theta_1^2 e^{-\gamma t}) \quad (\text{S15})$$

Allan deviations for this type of drift, shown in Fig. 3f, exhibit a characteristic transition between  $\sigma_{\omega} \propto \sqrt{1/\tau}$  (white noise) at short times and  $\sigma_{\omega} \propto \tau$  at long times, with a minimum that depends on  $\alpha_{\text{NL}}$ ,  $\theta_1$  and the total measurement time  $\tau_m$ . Here we derive an analytical expression for these curves.

Suppose an oscillator's frequency is measured for duration  $\tau_M$  at sampling rate of  $\Delta t^{-1}$ . Each fractional frequency measurement  $y_i = \omega_i / \omega_0$  has corresponding time  $t_i = (i-1)\Delta t$ , where  $i$  runs from 1 to  $M$  and  $M = \tau_M / \Delta t$  is the number of measurements. The Allan variance as a function of averaging time  $\tau$  can be estimated by averaging  $n = \tau / \Delta t$  adjacent frequency measurements. The Allan variance (estimator) is

$$\hat{\sigma}_y^2(n\Delta t) = \frac{1}{2n(M-2n+1)} \sum_{j=1}^{M-2n+1} \left( \sum_{i=nj}^{nj+n-1} y_{i+n} - y_i \right)^2. \quad (\text{S16})$$

During an amplitude ringdown  $\theta_0(t) = \theta_1 e^{-\gamma t/2}$ , assuming  $\gamma \ll \Delta t^{-1}$  (high  $Q$ ),  $\theta_i \approx \theta(t_i)$  and Eq. S15 can be written

$$y_i = 1 + \frac{\Delta\omega_1}{\omega_0} e^{-\gamma t_i}, \quad (\text{S17})$$

where  $\Delta\omega_i \equiv \omega_i - \omega_0 = \omega_0 \alpha_{\text{NL}} \theta_i^2$  is the initial frequency shift.

Plugging Eq. S17 into the Eq. S16 yields

$$\hat{\sigma}_y^2(\tau) = \left( \frac{\Delta\omega_1}{\omega_0} \right)^2 \frac{\Delta t^2 e^{2\gamma\Delta t}}{2\tau(\tau_M - 2\tau + \Delta t)} \times \dots \\ \times \frac{(1 - e^{-\gamma\tau})^4}{(e^{-\gamma\Delta t} - 1)^2} \frac{(1 - e^{-2\gamma(\tau_M - 2\tau + \Delta t)})}{e^{2\gamma\tau} - 1} \quad (\text{S18})$$

On short intervals, the ringdown resembles a linear frequency drift  $\Delta\omega_i \approx \Delta\omega_1(1 - \gamma t_i)$  corresponds to an Allan deviation

$$\sigma_y^{\text{NL}}(\tau) \approx \frac{|\Delta\omega_1|}{Q\sqrt{2}} \tau \quad (\text{S19})$$

as can be seen from Eq. S18 assuming  $\{\Delta t, \tau, \tau_M\} \ll \gamma^{-1}$ .

The stability of the oscillator in free decay is therefore limited by both thermal noise (Eq. S13),  $\sigma_y \sim \sqrt{1/\tau}$  and amplitude drift (S18)  $\sigma_y \sim \sqrt{\tau}$ . This gives rise to a minimum

$$\sigma_y(\tau_{\text{min}}) = \sqrt{\frac{3}{2}} \left( \frac{\Delta\omega_1}{2\omega_0\varepsilon Q^2} \right)^{1/3} = \sqrt{\frac{3}{2}} \left( \frac{\alpha_{\text{NL}}\theta_{\text{th}}^2}{Q^2} \right)^{1/3} \quad (\text{S20})$$

at averaging time

$$\tau_{\text{min}} = \left( \frac{Q}{2\varepsilon\omega_0\Delta\omega_1^2} \right)^{1/3} = \left( \frac{\theta_{\text{th}}^2 Q}{\alpha_{\text{NL}}^2 \omega_0^3 \theta_1^6} \right)^{1/3}. \quad (\text{S21})$$

## DEVICE IMAGES

Additional images of the micropendulum device shown in Fig. 1b are shown in Fig. S1. The 25- $\mu\text{m}$ -wide, 75-nm-thick  $\text{Si}_3\text{N}_4$  ribbon suspension spans a 5 mm  $\times$  5 mm window inside

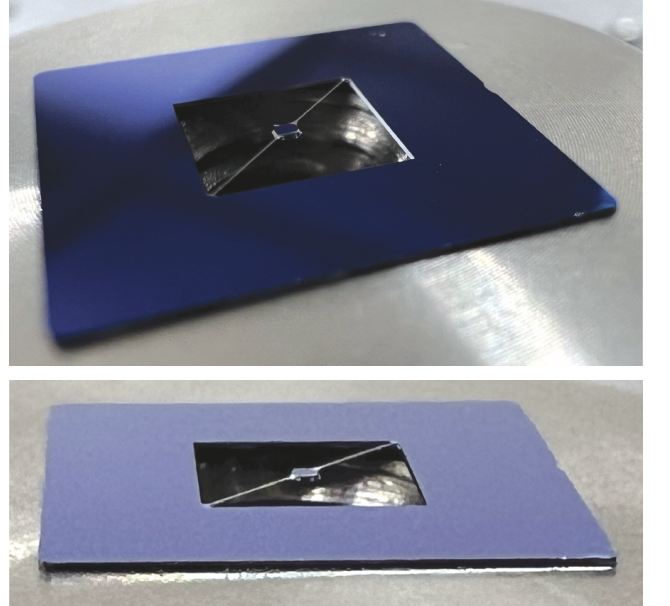


FIG. S1. Additional images of device in Fig. 1b.

of a  $12\text{ mm} \times 12\text{ mm}$  wide,  $200\text{-}\mu\text{m}$ -thick Si chip. Visible defects in the pad geometry are due to the non-uniformity of the KOH etch used to release the suspension. (Details of the fabrication procedure are described in the appendix of [6].) We have devised a new fabrication method employing deep reactive ion etching to more precisely define the pad dimensions (important for tailoring  $\alpha_{\text{NL}}$ ); however, we have found that the KOH-etched devices reported here and in [6] have similar  $Q$ .

### FREQUENCY SENSITIVITY TO TEMPERATURE

To determine the sensitivity of the micropendulum's frequency to temperature, frequency and temperature time series for both free-running (Fig. 3g) and self-sustained (Fig. 3g) oscillators were plotted against one another and fit to a line, as shown in S2. The fitted slope of the datasets gives  $df/dT = 0.070\text{ Hz/K}$  and  $0.067\text{ Hz/K}$ , respectively.

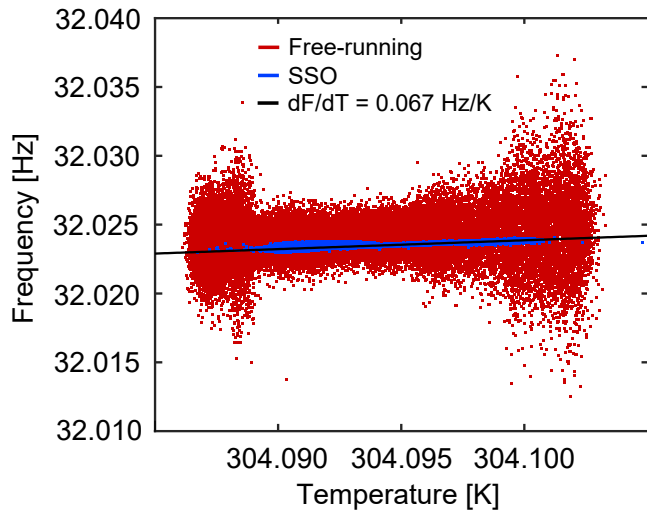


FIG. S2. Parametric plot of frequency  $f$  versus temperature  $T$  for free-running and self-sustained oscillator (SSO) measurements in Fig. 3. Linear fit to the SSO and free-runnings measurements yield  $df/dT = 0.067\text{ Hz/K}$  and  $0.070\text{ Hz/K}$ , respectively

### NONLINEAR STIFFNESS VERSUS SUSPENSION WIDTH

Figure 4 shows frequency versus amplitude measurements for devices with three different ribbon suspension widths,  $w$ . The  $w = 50\text{ }\mu\text{m}$  and  $w = 100\text{ }\mu\text{m}$  devices are the same as studied in [6]. The  $w = 25\text{ }\mu\text{m}$  device is a new sample fabricated for this study. To obtain the sensitivity estimates in Fig. 4b, we record the  $Q$  and the inverted frequency of each device via ringdown and thermal noise spectra, respectively, as shown in Fig. S1. Note that the  $Q$  factors have degraded relative to their original values [6], likely due to contamination while in storage or transit between vacuum chambers. We therefore use

the original values in Fig. 4b.

As mentioned in the main text, we have devised a strategy to balance the pendulum and suspension nonlinearity while preserving gravitational sensitivity, by carefully controlling the dimensions of the torsion paddle and ribbon suspensions. A new fabrication process employing deep reactive ion etching has allowed us to realize  $100\text{ Hz}$  micropendula with  $\alpha_{\text{NL}} = 10^{-3}$  and  $R \geq 5\text{ Hz}/g_0$ . The limits of this process are currently being explored.

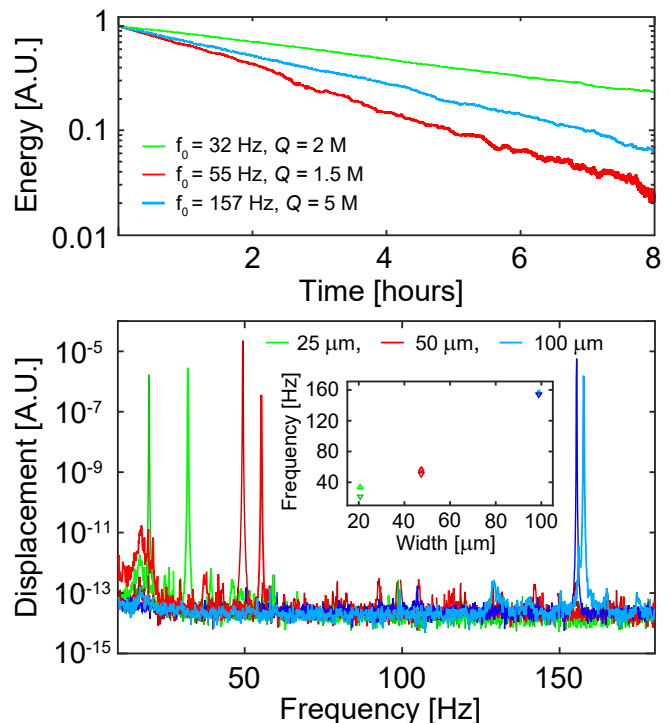


FIG. S3. (top) Energy ringdowns of the three micropendula used in Fig. 4 in the main text. (bottom) Displacement spectra of each in their normal (light colors) and inverted (dark colors) configuration. Inset: Frequency of each pendulum in both configurations, as a function of ribbon suspension width.

- [1] J. R. Pratt, S. Schlamminger, A. R. Agrawal, C. A. Condos, C. M. Pluchar, and D. J. Wilson, in *ICND* (Springer, 2023) pp. 3–14.
- [2] R. H. Rand (2012).
- [3] P. Sadeghi, A. Demir, L. G. Villanueva, H. Kähler, and S. Schmid, *Physical Review B* **102**, 214106 (2020).
- [4] M. Wang, R. Zhang, R. Ilic, V. Aksyuk, and Y. Liu, *Nano letters* **20**, 3050 (2020).
- [5] A. Demir, *Journal of Applied Physics* **129** (2021).
- [6] J. R. Pratt, A. R. Agrawal, C. A. Condos, C. M. Pluchar, S. Schlamminger, and D. J. Wilson, *Phys. Rev. X* **13**, 011018 (2023).